Dual phase $Li_4Ti_5O_{12}$-TiO_2 hierarchical hollow microspheres as anode materials for high rate lithium-ion batteries

Kunxu Zhu and Guoxin Hu[1]

School of Mechanical & Power Engineering, Shanghai Jiao Tong University, Shanghai 200240, P.R. China

E-mail: hugx@sjtu.edu.cn

Abstract.Dual phase $Li_4Ti_5O_{12}$-TiO_2 hierarchical hollow microspheres composed of nanosheets are successfully fabricated by the calcination of hydrothermal product obtained from lithium peroxotitanate complex solution. Low-cost industrial H_2TiO_3 particles are chosen as titanium sources, which is significant for the inexpensive and large-scale production of $Li_4Ti_5O_{12}$-TiO_2 composite material. The $Li_4Ti_5O_{12}$-TiO_2 electrode yields excellent rate capability (151, 139 and 134 mA h g^{-1} at 10, 20 and 25 C, respectively) and good cycling stability (96% capacity retention after 500 cycles at 10 C). The mesoporous hierarchical morphology and high grain boundary density are likely the contributing factors to the excellent electrochemical performance of $Li_4Ti_5O_{12}$-TiO_2 composite.

1. Introduction

Rechargeable lithium ion batteries (LIBs) have been used as the energy sources for most portable electronic devices due to their large energy density and long cycle life, whereas their practical application in electric vehicles (EVs) and stationary energy storage systems highly depends on the electrochemical performance of electrode materials, such as large capacity, high power and energy density, and good cycling stability [1, 2]. Graphite-based materials are currently the dominant anode materials for commercial LIBs, however, poor rate performance resulted from their low Li^+ diffusion coefficient, serious safety issues induced by lithium dendrite formation when the Li-insertion potential approaches almost 0 V vs. Li/Li^+, and poor cycle stability caused by volume change (ca. 9-13%) during lithiation/delithiation processes limits their applications for the next generation high power and energy LIBs [3-5].

Among different mushrooming advanced materials that substitute the traditional carbonaceous anode materials, titanium oxide based materials (e.g., $Li_4Ti_5O_{12}$ and TiO_2) have been proven to be the potential alternative anode materials for LIBs because they are inherently safe and compatible with the electrolyte [6, 7]. Spinel $Li_4Ti_5O_{12}$ (LTO) features a stable operating voltage plateau of about 1.55 V vs. Li/Li^+, which is high enough to avoid most electrolyte reduction and thus enhances the safety performance. Also, as a “zero-strain” material, LTO has excellent structural stability with negligible volume change during Li^+ insertion/extraction process, which results in the good reversibility and cycling stability. So LTO was the first commercialized non-carbonaceous anode material for LIBs in EVs and advanced energy storage devices by companies such as Toshiba [8, 9] and Altairnano [10]. Nevertheless, the drawbacks of LTO should not be ignored, i.e., the intrinsic low electronic conductivity (ca. 10^{-13} S cm^{-1}) and poor lithium ion diffusion coefficient (10^{-9}-10^{-12} cm^2 s^{-1}) restrict the rate capability of LTO.

So far, many efforts have been made to improve the rate performance of LTO, such as surface conductive coating [11-13], doping with heteroatoms [14, 15], and preparing nanostructured LTO materials [16-18]. Among these approaches, preparing LTO nanomaterials is an attractive and efficient way, because reducing LTO particle size to nanometer scale significantly shortens the electrons/lithium ions transport length and increases the contact area between active material and electrolyte. On the other hand, interfacial design has been demonstrated another way to improve the lithium ion transport properties and electronic conductivity of the electrode material [19, 20]. When the spacing of interfaces is reduced down to the nanoscale regime, the grain boundaries would act as channels to transport electrons and lithium ions in the particles. And the grain boundaries with large interfacial areas can store a large number of lithium ions, increasing the specific capacities of the materials [21]. Therefore, LTO materials featuring a high boundary density with large interfacial areas are expected to improve their rate capability. To increase grain boundary density, it is reasonable to choose dual- or multi-phase compounds rather than single phase compounds. This is consistent with several recent reports that dual phase $Li_4Ti_5O_{12}$-TiO_2 materials showed excellent electrochemical performance as anode materials for LIBs [22-24].

Herein, our purpose was to combine the advantages of both nanostructure and dual phase to improve the electrochemical performance of LTO. Instead of using organometallic titanium compounds such as tetrabutyl titanate or titanium isopropoxide as Ti sources, we chose low-cost and abundant industrial H_2TiO_3 particles to supply Ti element, which occupies more than 52.2% mass percentage in $Li_4Ti_5O_{12}$-TiO_2 composite. This is significant for the inexpensive and large-scale production of $Li_4Ti_5O_{12}$-TiO_2 nanomaterials. By dissolving H_2TiO_3 particles in LiOH solution with the help of H_2O_2, peroxotitanate complex solution was obtained. Dual phase $Li_4Ti_5O_{12}$-TiO_2 hierarchical hollow spheres composed of nanosheets were finally prepared by calcining the hydrothermal product from the peroxotitanate solution. The $Li_4Ti_5O_{12}$-TiO_2 composite electrode showed excellent electrochemical performance.

2. Experimental

2.1 Materials synthesis

The $Li_4Ti_5O_{12}$-TiO_2 materials were synthesized by a hydrothermal reaction of peroxotitanate complex precursor solution followed by a calcination treatment. The precursor solution was obtained by the same way reported in our previous work [25, 26]. Typically, 1.0 g of $LiOH{\cdot}H_2O$ was dissolved in 20 ml deionized water. 1.3 g of commercial H_2TiO_3 powder (ca. 1 μm in diameter) and 8 ml of H_2O_2 (30%) were then added into the solution. After magnetic stirring for 1.5 h at 33 °C, a pale yellow solution was obtained and then transferred into a 50 ml Teflon-lined stainless steel autoclave, which was subsequently heated at 110 °C for 6 h. After cooling down naturally, the white precipitate was filtered and washed by deionized water several times, and then dried at 80 °C for 3 h. Finally, the dried powders were calcined at 550 °C for 4 h to obtain the $Li_4Ti_5O_{12}$-TiO_2 materials.

2.2 Materials characterization

The phase compositions of the samples were identified by X-ray diffraction (XRD, D8 Advance, Bruker) with Cu K_a (λ = 0.15418 nm) radiation. The morphologies were characterized using field emission scanning electron microscope (FE-SEM, JEOL JSM-7800F Prime) and transmission electron microscope (TEM, JEOL JEM-2100, 200Kv). The nitrogen adsorption/desorption isotherms were obtained by a Micromeritics TriStar II 3020 apparatus.

2.3 Electrochemical measurement

The working electrodes were prepared by mixing the active materials, carbon black, and polyvinylidene difluoride (PVDF) at a weight ratio of 80: 10: 10 in *N*-methylpyrrolidone (NMP). The obtained slurry was coated onto a Cu foil and vacuum dried at 80 °C for 12 h, and then cut into disks. The electrochemical measurements were carried out using CR2032 coin-type cells which were

assembled in an Ar-filled glove box (H_2O, O_2< 1 ppm), with lithium metal as the counter electrode, Celgard 2400 as the separator, and 1M $LiPF_6$ in a mixture of ethylene carbonate (EC)/dimethyl carbonate(DMC) (1/1 in volume) as the electrolyte. Galvanostatic charge/discharge cycles of the cells were tested between 1.0 and 3.0 V vs. Li/Li^+ on a Land CT2001A battery tester. Cyclic voltammetry (CV) measurement was performed on a CHI 660D electrochemical workstation.

3. Results and Discussion

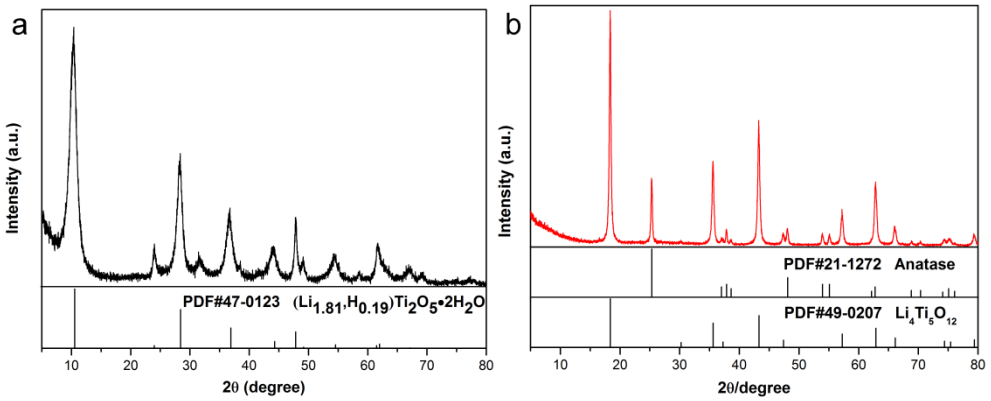

Figure 1. XRD patterns of (a) hydrothermal product obtained from peroxotitanate complex solution and (b) as-prepared $Li_4Ti_5O_{12}$-TiO_2 composite material.

H_2TiO_3 particles with poor crystallinity were easily dissolved in the LiOH solution in the presence of H_2O_2 to form peroxotitanate complex solution. Figure 1a shows the XRD pattern of hydrothermal product obtained from the peroxotitanate precursor solution, which is ascribed to layered lithium titanate $Li_{1.81}H_{0.19}Ti_2O_5 \cdot 2H_2O$ (JCPDS NO. 47-0123) [22]. After calcined at 550 °C in the air, $Li_4Ti_5O_{12}$ with a cubic spinel structure (JCPDS NO. 49-0207) as well as anatase TiO_2 (JCPDS NO. 21-1272) were detected in the product, as presented in figure 1b. The XRD analysis confirms that both spinel $Li_4Ti_5O_{12}$ and anatase TiO_2 exist in the calcined product, forming a dual-phase $Li_4Ti_5O_{12}$-TiO_2 composite material. The formation of anatase TiO_2 may be caused by the crystallization of residual amorphous titania in the hydrothermal product. Moreover, the weight percent of the spinel $Li_4Ti_5O_{12}$ is caculated about 84.9% according to the XRD pattern.

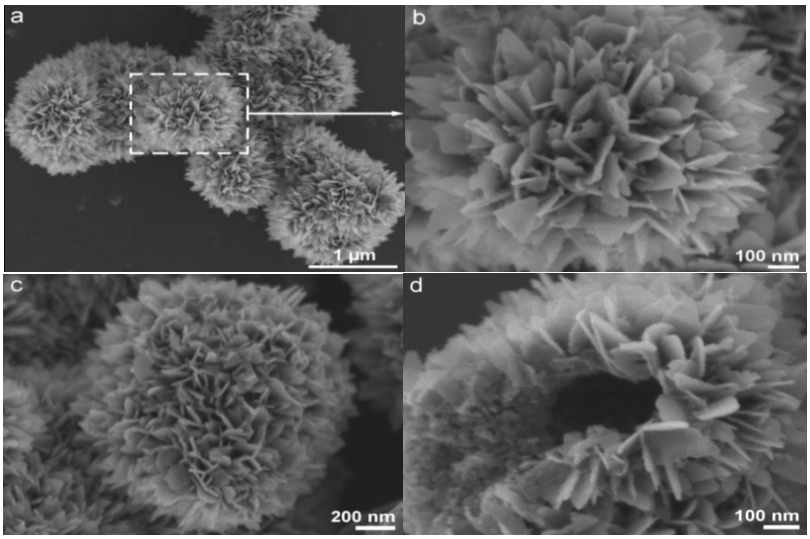

Figure 2. SEM images of (a, b) $Li_{1.81}H_{0.19}Ti_2O_5 \cdot 2H_2O$ hierarchical hollow microspheres and (c, d) $Li_4Ti_5O_{12}$-TiO_2 hierarchical hollow microspheres.

The morphologies of the $Li_{1.81}H_{0.19}Ti_2O_5 \cdot 2H_2O$ and $Li_4Ti_5O_{12}$-TiO_2 products were revealed by SEM and TEM observations. SEM images in figure 2a and b show that the $Li_{1.81}H_{0.19}Ti_2O_5 \cdot 2H_2O$ lithium titanate exhibits a hierarchical sphere-shaped morphology assembled by primary interleaving nanosheets. The diameters of the microspheres are around 1.2 μm and the thickness of nanosheets ranges from 10 to 20 nm. Actually, these spheres are hollow inside, as is shown in figure 3a. The assembly of the nanosheets results in the formation of the large interior void space and the well-defined shell. Although calcined at 550 °C for 4 hours, the $Li_4Ti_5O_{12}$-TiO_2 sample still retains the initial microstructures of the hydrothermal product, as presented in figure 2c. And the inside hollow structure of the $Li_4Ti_5O_{12}$-TiO_2 sample is confirmed by a cross section of a damaged microsphere (figure 2d).

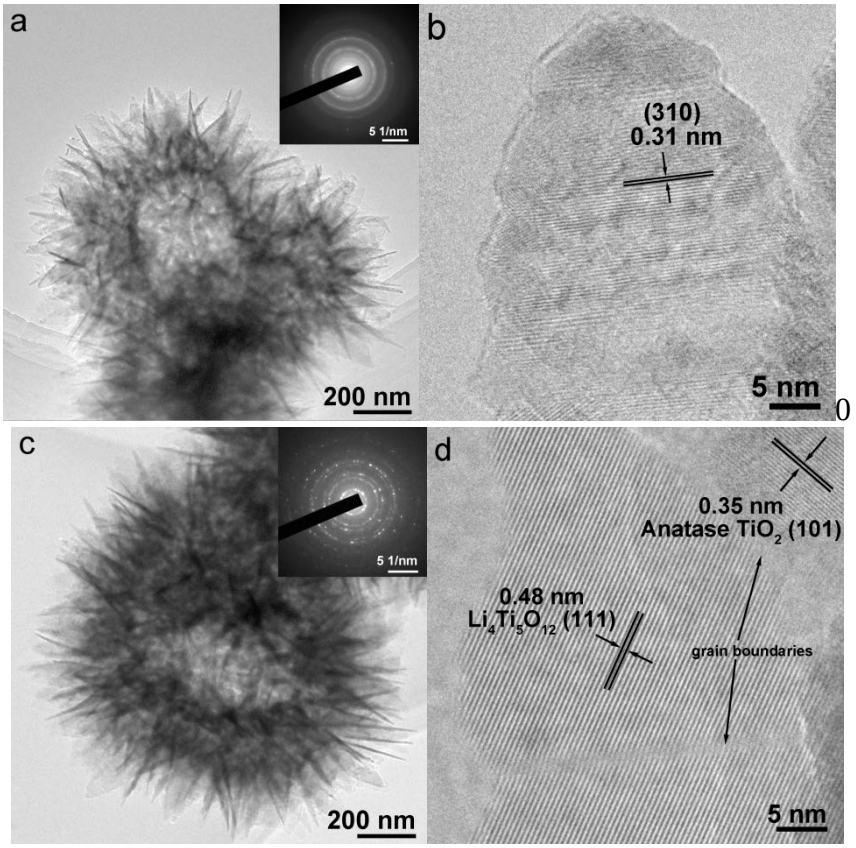

Figure 3. TEM images of (a, b) $Li_{1.81}H_{0.19}Ti_2O_5 \cdot 2H_2O$ hierarchical hollow microspheres and (c, d) $Li_4Ti_5O_{12}$-TiO_2 hierarchical hollow microspheres.

Figure 3 shows further structural features of the hydrothermal and calcined products. A typical single nanosheet of the $Li_{1.81}H_{0.19}Ti_2O_5 \cdot 2H_2O$ microsphere (figure 3a) has a length of approximately 200 nm and width of 70-110 nm. A top view HRTEM image of a nanosheet in figure 3b exhibits a lattice spacing of 0.31 nm, which is assigned to (310) plane of $Li_{1.81}H_{0.19}Ti_2O_5 \cdot 2H_2O$, consistent with the XRD result. For $Li_4Ti_5O_{12}$-TiO_2 material, negligible change to the hierarchical hollow sphere-shaped structure indicates a good structural stability of the spheres (figure 3c). It should be mentioned that the primary nanosheets can be destroyed into particle aggregates when calcined at higher temperature (700 °C). A top view TEM image shown in figure 3d reveals the crystal structure of the nanosheets. Two sets of lattice fringe spacing of 0.48 and 0.35 nm are observed, which are ascribed to the (111) plane of $Li_4Ti_5O_{12}$ and (101) plane of anatase TiO_2, respectively, confirming the coexisting phases of $Li_4Ti_5O_{12}$ and TiO_2 in the sample. Moreover, some grain boundaries are observed among

the crystalline domains in the nanosheets, which are considered beneficial for the improvement of lithium ions and electrons transport.

Figure 4 shows the N_2 adsorption/desorption isotherms of the $Li_4Ti_5O_{12}$-TiO_2 hierarchical hollow microspheres. A typical Ⅳ curves with an H1 hysteresis loop is observed for this sample, indicating that the $Li_4Ti_5O_{12}$-TiO_2 material has open mesoporous structures. The inset in figure 4 is the pore size distribution curve calculated by Barrett-Joyner-Halenda (BJH) method. The dual phase $Li_4Ti_5O_{12}$-TiO_2 microspheres exhibit a pore size distribution with an average pore diameter at ca. 20 nm. The $Li_4Ti_5O_{12}$-TiO_2 microspheres have a Brunauer-Emmett-Teller (BET) specific surface area of 51 m^2 g^{-1} and a pore volume of 0.26 m^3 g^{-1}. Hereby, depending on the demonstrated structural features, the $Li_4Ti_5O_{12}$-TiO_2 hierarchical hollow microspheres are expected to make the contact between active material and electrolyte more efficiently and shorten the electrons/lithium ions transport length, thus enhancing the electrochemical performance.

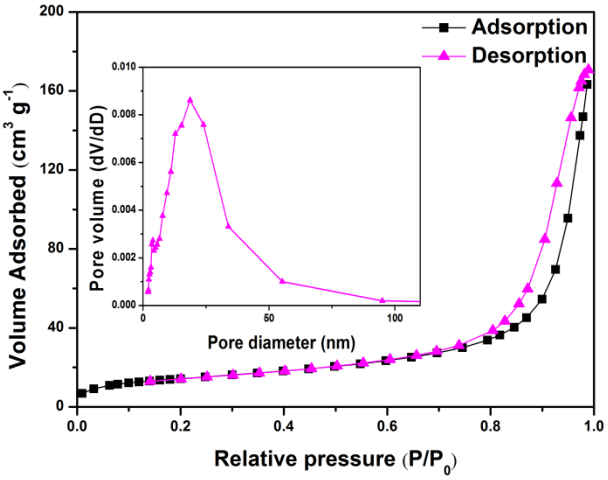

Figure 4. Nitrogen adsorption-desorption isotherms of the $Li_4Ti_5O_{12}$-TiO_2 microspheres. The inset is the pore size distribution calculated by BJH method.

The electrochemical performance of the dual phase $Li_4Ti_5O_{12}$-TiO_2 materials was evaluated by coin-type cells, using metallic lithium foil as both counter and reference electrodes. Figure 5a shows the first two CV cycles conducted between 1.0 and 3.0 V at a scan rate of 0.2 mV s^{-1}. In the first cycle, two pairs of redox peaks located at 1.435/1.697 V and 1.668/2.054 V (vs. Li/Li^+) are associated with Li^+ insertion/extraction within the spinel $Li_4Ti_5O_{12}$ and anatase TiO_2, respectively. In the second cycle, the curve shape and redox peak potentials are substantially unchanged, and the redox peaks have good symmetry, suggesting excellent reversibility and high coulombic efficiency of the $Li_4Ti_5O_{12}$-TiO_2 electrode [14, 17, 22].

Figure 5b presents the galvanostatic discharge-charge curves of the $Li_4Ti_5O_{12}$-TiO_2 electrode at C-rates of 0.5-25 C (1C = 175 mA g^{-1}). At relatively low rates (0.5, 1, 2 C), besides a voltage platform around 1.55 V (vs. Li/Li^+) related to Li^+ insertion/extraction in spinel $Li_4Ti_5O_{12}$, a voltage plateau at around 1.7 and 2.0 V is observed, which is the characteristic of Li^+ ion insertion/extraction of anatase TiO_2. The $Li_4Ti_5O_{12}$-TiO_2 materials can deliver a discharge capacity of 181, 174, 165, 157, 151, 139, 134 mA h g^{-1} when cycled at rate of 0.5, 1, 2, 5, 10, 20, and 25 C, respectively. According to the rate performance in figure 5c, when the rate is put back to 0.5 C, the discharge capacity of the $Li_4Ti_5O_{12}$-TiO_2 electrode returns back to 180 mA h g^{-1}, which further confirms the excellent reversibility of the $Li_4Ti_5O_{12}$-TiO_2 electrode. The capacities of $Li_4Ti_5O_{12}$-TiO_2 are much higher than the compared commercial $Li_4Ti_5O_{12}$ sample, especially at high rates, which only delivers discharge capacity of 165, 140, 111, 82, 50, 32 and 25 mA h g^{-1} at 0.5, 1, 2, 5, 10, 20 and 25 C, respectively. In addition, the $Li_4Ti_5O_{12}$-TiO_2 electrode exhibits an outstanding cycling stability over long-term cycles at high rate

of 10 C. As shown in figure 5d, the $Li_4Ti_5O_{12}$-TiO_2 electrode gives a discharge capacity of 145 mA h g^{-1} after 500 cycles, which is 96% of the initial 151 mA h g^{-1}. The periodic fluctuation of the charge/discharge capacity is caused by the temperature difference between day and night. And the coulombic efficiency reaches to 100% after the first two cycles, confirming the great cycling stability of the material.

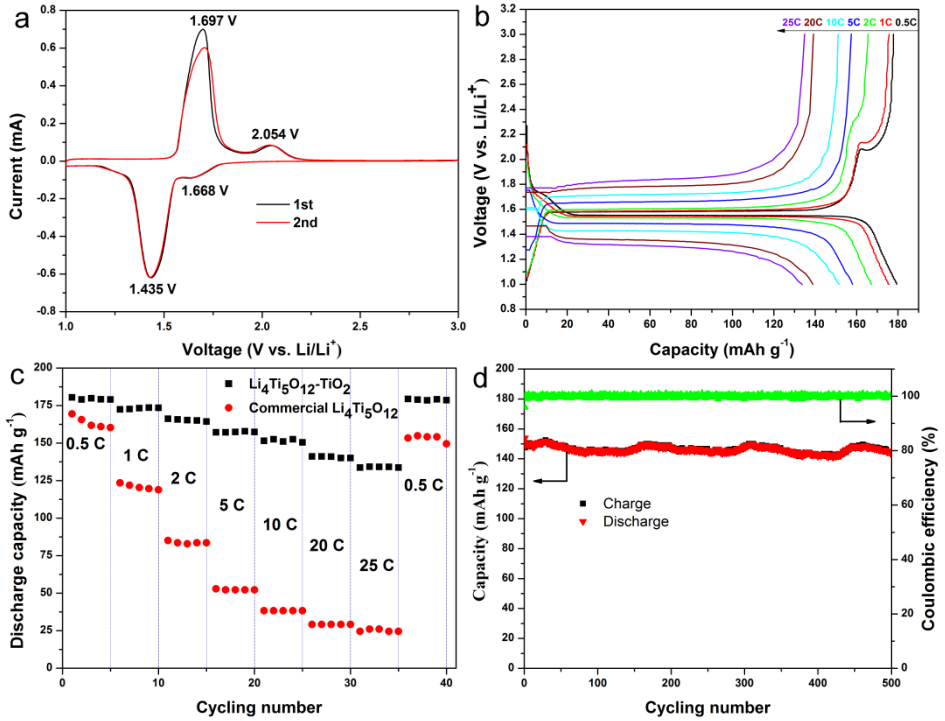

Figure 5. (a) The initial two CV curves of the dual phase $Li_4Ti_5O_{12}$-TiO_2 electrode obtained at a scan rate of 0.2 mV s^{-1}; (b) the galvanostatic discharge-charge profiles of the $Li_4Ti_5O_{12}$-TiO_2 electrode at different C-rates from 0.5 to 25 C; (c) Rate performances of the $Li_4Ti_5O_{12}$-TiO_2 electrode and commercial $Li_4Ti_5O_{12}$ electrode at rates of 0.5-25 C; (d) cycling performance of $Li_4Ti_5O_{12}$-TiO_2 electrode and the corresponding coulombic efficiency at a rate of 10 C; All the electrochemical measurements were conducted within a voltage window of 1.0-3.0 V (vs. Li/Li^+).

4. Conclusion

In conclusion, we have successfully prepared dual phase $Li_4Ti_5O_{12}$-TiO_2 hierarchical hollow microspheres assembled by nanosheets through hydrothermal treatment of peroxotitanate complex solution and a followed calcination. The dual phase composition of the $Li_4Ti_5O_{12}$-TiO_2 material results in the formation of some grain boundaries among the crystalline domains in the nanosheets. Combining with the unique mesoporous hierarchical nanostructure, the $Li_4Ti_5O_{12}$-TiO_2 electrode exhibits excellent rate capability (134 mA h g^{-1} at 25 C) and cycling stability (145 mA h g^{-1} retained after 500 cycles at 10 C). Furthermore, instead of organometallic titanium compounds, industrial low-cost H_2TiO_3 particles were chosen as the Ti sources, which is significant for the inexpensive and large-scale production of the $Li_4Ti_5O_{12}$-TiO_2 materials.

Acknowledgement

This work was supported by the National Natural Science Foundation of China (No. 51476100, 51676128 and 51506124). The authors thank the Instrumental Analysis Center of Shanghai Jiao Tong University (SJTU) for SEM measurements.

References

[1] Tang Y, Zhang Y, Li W, Ma B and Chen X 2015 *Chem. Soc. Rev.* **44** 5926-40
[2] Choi J W and Aurbach D 2016 *Nat. Rev. Mater.* **1** 16013
[3] Shen L, Uchaker E, Zhang X and Cao G 2012 *Adv. Mater.* **24** 6502-6
[4] Xu H, Hu X, Sun Y, Luo W, Chen C, Liu Y and Huang Y 2014 *Nano Energy* **10** 163-71
[5] Shi Y, Gao J, Abruña H D, Liu H, Li H, Wang J and Wu Y 2014 *Nano Energy* **8** 297-304
[6] Zhu G N, Wang Y G and Xia Y Y 2012 *Energy Environ. Sci.* **5** 6652-67
[7] Yi T F, Yang S Y and Xie Y 2015 *J. Mater. Chem.* **3** 5750-77
[8] Takami N, Kosugi S and Honda K 2008 *Toshiba Rev.* **63** 54-7
[9] Toshiba, Toshiba's SCiB™ Rechargeable Battery, *http://www.scib.jp/en/index.htm*.
[10] Manev V, Spitler T, Stewart M and Shelburne J 2010 Negative electrode for lithium ion battery. In: Altairnano, editor.: *Google Patents*.
[11] Li B, Han C, He Y B, Yang C, Du H, Yang Q H and Kang F 2012 *Energy Environ. Sci.* **5** 9595-602
[12] Ma Y, Ding B, Ji G and Lee J Y 2013 *ACS Nano* **7** 10870-8
[13] Sha Y, Xu X, Li L, Cai R and Shao Z 2016 J. *Power Sources* **314** 18-27
[14] Chen C, Huang Y, An C, Zhang H, Wang Y, Jiao L and Yuan H 2015 *ChemSusChem* **8** 114-22
[15] Kim J G, Shi D, Park M S, Jeong G, Heo Y U, Seo M, Kim Y J, Kim J H and Dou S X 2013 *Nano Res.* **6** 365-72
[16] Chen J, Yang L, Fang S and Tang Y 2010 *Electrochim. Acta* **55** 6596-600
[17] Cheng J, Che R, Liang C, Liu J, Wang M and Xu J 2014 *Nano Res.* **7** 1043-53
[18] Haridas A K, Sharma C S and Rao T N 2015 *Small* **11** 290-4
[19] Liao J-Y, Chabot V, Gu M, Wang C, Xiao X and Chen Z 2014 *Nano Energy* **9** 383-91
[20] Rahman M M, Wang J-Z, Hassan M F, Wexler D and Liu H K 2011 *Adv. Energy Mater.* **1** 212-20
[21] Jiang Y M, Wang K X, Zhang H J, Wang J F and Chen J S 2013 *Sci. Rep.* **3** 3490-4.
[22] Jiang Y M, Wang K X, Wu X Y, Zhang H J, Bartlett B M and Chen J S 2014 *ACS Appl. Mater. Interfaces* **6** 19791-6
[23] Yi T F, Fang Z K, Xie Y, Zhu Y R and Yang S Y 2014 *ACS Appl. Mater. Interfaces* **6** 20205-13
[24] Xu C, Xue L, Zhang W, Fan X, Yan Y, Li Q, Huang Y and Zhang W 2014 *Electrochim. Acta* **147** 506-12
[25] Zhu K X and Hu G X 2014 *J. Supercrit. Fluids* **94** 165-73
[26] Zhu K X, Gao H Y, Hu G X, Liu M J and Wang H C 2017 *J. Power Sources* **340** 263-72